

CoNiCrMo, FeCrNi, NiCr and FeNiAlMo modified iron based alloy coating deposited by plasma transferred arc process

S. O. YILMAZ^a, T. TEKER^{b*}

^aUniversity of Firat, Faculty of Engineering, Department of Metallurgy and Materials Engineering, 23117, Elazığ, Turkey,

^bUniversity of Adiyaman, Faculty of Engineering, Department of Materials Engineering, 02040, Adiyaman, Turkey

The technique of alloying an X120Mn12 steel substrate with the plasma transferred arc process was used to develop a surface with high toughness and wear resistance in high temperature applications. Co, Cr, Al and Ni-intermetallic phases were formed inside an Fe-based composite surface coating. The phase transformations on these coated surfaces were comprehensively examined using a combination of scanning electron microscopy and energy dispersive spectrometry microanalysis. The microstructure studies of the superficial layers of the coating revealed an inter-dendritic austenite (γ) phase structure and fine eutectic Ni-based inter-metallics.

(Received September 8, 2011; accepted September 18, 2013)

Keywords: PTA, X120Mn12, Coating

1. Introduction

The plasma transferred arc (PTA) technique is a process that can be used for surface modification of steels using a low melting point and cheap ferroalloy powders. During the coating process, ferroalloy powders and a thin surface layer of the substrate material are melted together and then rapidly solidified to form a dense coating that metallurgically bonds with the base material. The PTA process is widely used for the surface treatment of materials and was developed as a modification of the plasma arc welding method [1-5]. It uses the basic principles used in traditional welding surfacing techniques, but provides a higher deposition. The surfacing process is characterized by extremely high temperature, excellent arc stability, low thermal distortion of the part and high coating speeds [6]. The process has the advantage of using two independent arcs (namely the non-transferred arc as the pilot and the transferred arc as the main arc), where argon gas is passed between a cathode and an anode, and an ionized constricted plasma arc is formed. The ionized gas provides a path for the transferred arc [6,7] and then the coatings can be produced by synthesizing Fe-, Co-, and Ni-based alloy coatings on various traditional substrate materials [7,8]. This technique has the potential to produce rapidly-solidifying fine microstructures that exhibit high hardness and increased wear resistance. This type of microstructure possesses good tribological properties [9-12], and the microstructures of coated surfaces with a high chromium content are expected to have homogeneously distributed intermetallic phases in these microstructures.

Ni-Fe-Mn-Co-Cr-Al alloy systems are known to establish a dual-phase microstructure of γ -Ni, Co, Mn and β -NiAl phase with occasional γ -Ni₃Al and α -Cr, Fe, Mo

phases as dispersal from the fully processed state [13]. The solidification rate of MCrAl coatings can be a critical issue. Metastable phases, single-phase crystalline and amorphous coatings, however, may be advised for some corrosive environments. The manufacture of phase structures through solidification is facilitated in systems that provide an invariant reaction on solidification. In a Ni-Co-Mn-Cr-Mo-Fe-Al system, however, the reaction of liquid to γ -(Ni, Co, Mn) + α -(Cr, Mo, Fe) + β -(Ni, Co, Mn)Al is still to solidify over the melting range, whereas an invariant eutectic reaction of the above scheme is typical for a ternary system such as the Ni-Cr-Al system.

The newly-formed coated surfaces were investigated by changing the alloying elements (Cr, W, Ni, Al, Mo), the size of the dendrites, the eutectic reaction temperatures, the hardness and the coating thickness, as well as the processing parameters (powder feed rate and heat input). It aimed to produce a hard, tough, wear-resistant MMC coating using the PTA process on high Mn steel under different conditions. PTA was used as a high-energy density beam to create a surface containing intermetallics in an austenite phase on X120Mn12 steel using Co, FeCrNi, NiCr and FeNiAlMo powders.

2. Experimental procedures

Rectangular plates of the steel (X120Mn12, 127 mm long, 51 mm wide and 9 mm thick) were used as substrates in the PTA processing experiments. The steel was in a soft annealed condition with a hardness of 180 HV. The chemical compositions of the Co, FeCrNi, NiCr and FeNiAlMo powders used as the surfacing alloys are given in Table 1. The experimental conditions employed are

listed in Table 2. A standard microhardness tester equipped with a Vickers indenter and a 5 g indentation load was used to measure the microhardness of polished surfaces and subsurfaces.

Table 1. Chemical composition of the powders used for coating.

	Cr	Fe	Co	Mo	Ni	Al
CoNiCrMo	5	-	Bal.	1	8	-
FeCrNi	20.56	Bal.	0.2	0.8	10	-
NiCr	26.7	-	-	-	73.0	0.
						3
FeNiAlMo	3.5	Bal.	-	3.2	20.0	6.
						0

Table 2. PTA operating parameters.

Transferred arc current	85–220 A
Transferred arc voltage	36–38 V
Torch gap	7 mm
Ion gas flow	0.5 m ³ /h
Travel speed	105 mm/min
Oscillation rate	21 times/min
Powder supply	0.2-1.5 g/s

Table 3. Effect of processing parameters on the coating geometry and microhardness.

Sample	Process parameters		Coating Dimensions (μm)				Coating characters	
	Powder Feed Rate (g/s)	Heat input (J/cm ²)	d _c	h _c	t _c	w _c	HV(kg _f /mm ²)	γ /vol.
FeCrNi								
S _{1.1}	0.2	5	110	710	820	6280	1120	0.15
S _{1.2}	1	10	330	1430	1760	7600	1170	0.20
S _{1.3}	1.5	22	1420	740	2160	7100	1345	0.27
NiCr								
S _{2.1}	0.2	5	28	2150	2178	6660	775	0.21
S _{2.2}	1	10	115	2650	2765	8200	893	0.24
S _{2.3}	1.5	22	1300	1750	3050	9650	995	0.38
FeNiAlMo								
S _{3.1}	0.5	5	170	420	590	5130	709	0.16
S _{3.2}	1	10	430	1200	1630	6540	782	0.22
S _{3.3}	1.5	22	810	1860	2670	9300	865	0.34
CoNiCrMo								
S _{4.1}	0.5	5	270	560	793	5640	598	0.12
S _{4.2}	1	10	530	900	1740	6820	622	0.19
S _{4.3}	1.5	22	850	1260	2270	9930	665	0.21

d_c = max depth below the original substrate surface, h_c = max height above the original substrate surface, t_c = max total thickness (=d_c+h_c), w_c = max width

The first group of samples was coated using FeCrNi powder (Table 3). Fig. 1 shows the SEM micrograph of the superficial layer of sample S_{1.1}. The microstructure is judged to be a needle-like γ / arrangement. So, the two-

The microstructure of the samples was revealed by etching with a solution composed of 5 g FeCl₃, 30 ml HCl and 100 ml distilled water. The microstructural evolution was then studied using optical and scanning electron microscopes (SEM) (Model JSM-5310, Japan). Energy dispersive spectrometry (EDS) was used to study the concentrations of alloying elements in the coatings deposited by PTA-process. For the X-Ray diffraction (XRD) analysis, a Rigaku Geigerflex X-ray diffractometer operating at 40 kV and 30 mA using Cu-K α radiation was used.

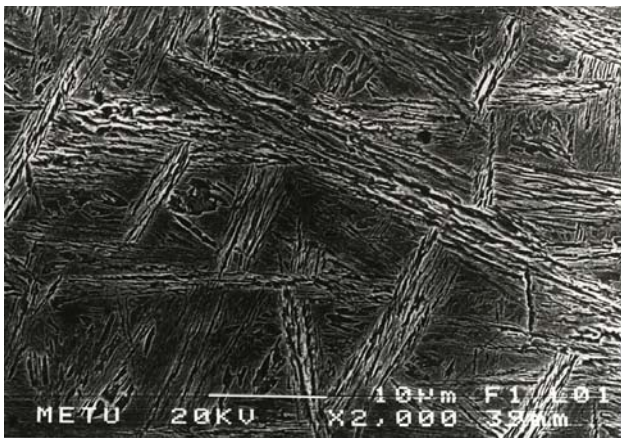
3. Results

3.1. Microstructural examination

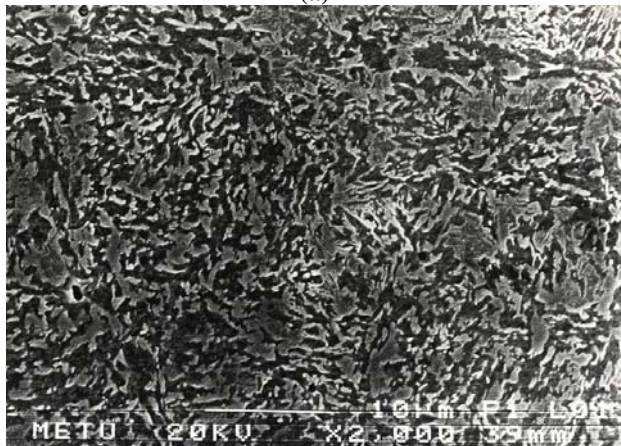
The physical properties of the coating for the different process parameters are listed in Table 3, which reveals the role of PTA processing parameters on the resulting dimensions, hardness, intermetallic vol.% and size of the coating. The alloyed depths of the coated surfaces were classified according to the power and powder feed rate and it was observed that the coating dimensions and hardness changed according to the process parameters and powder type.

phase grain represents a γ / γ / fibrous eutectic-like microstructure consisting of the two cubic phases. The stability of the γ -Ni₃Al phase in a system can thus be determined. γ / formation is a slow reaction, so if

superalloys are heated beyond γ/solvus and then cooled down too rapidly, $\gamma/\text{-Ni}_3\text{Al}$ forming will probably not show any $\gamma/$ precipitates. On the other hand, under extreme cooling rates $\gamma/$ melt compositions show metastable $\gamma/$ lattice arrangements [14], and primary solidification of $\gamma/$ from the melt becomes possible. The $\gamma/$ fibres grow perpendicular to the substrate surface, which means they run along the direction of solidification. The inter-centre spacing between the $\gamma/$ particles is roughly $0.1\ \mu\text{m}$ at the grain center and $0.05\ \mu\text{m}$ at the exterior, and their cross sections are of similar sizes. The diameter of this phase varies extensively, even in closely neighboring areas.



(a)



(b)

Fig. 1. SEM microstructure of a) Sample S_{1.1} (X2000),
b) Sample S_{1.3}.

Three points were chosen on the transverse section of the coated surface to determine the changes in the chemical composition from the surface to the substrate by EDS analysis (Fig. 1). It is observed from the micrograph that the intermetallic phases occupy an interdendritic form, and that the microstructure is in the form of a $(\text{CrFeNiSi} + \gamma'(\text{Ni}_3\text{Al}) + \gamma + \alpha')$ phase mixture.

The changes in the EDS analyses of the coated surface are shown in Fig. 2. The distribution of the elemental concentration is not homogenous; from the surface to the substrate, the Ni, Cr and Al concentrations were decreased.

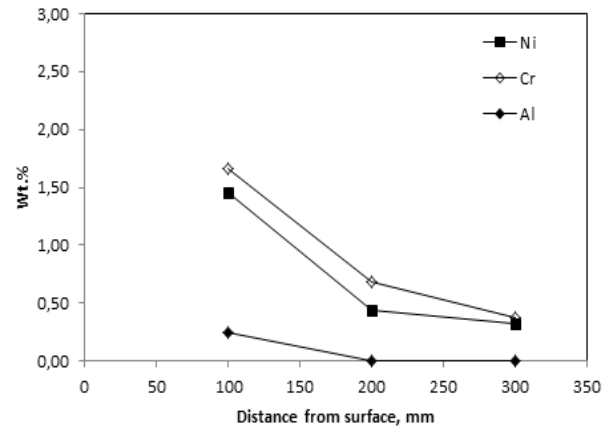


Fig. 2. Cross-Sectional elemental concentration of sample S_{1.1}.

Most of the Mn is dissolved in γ , but no Al is found in it. The portion of Mn to Ni is slightly higher than in the average alloy concentration. On the other hand, the proportion of Mn to Ni in $\gamma/$ is nearly zero in order to maintain a balance in the distribution of elements in both phases. The difference in concentration between γ and $\gamma/$ was approximately 60%. The difference of 50% found in the present study is too high to account for a sluggish volume-diffusion driven precipitation reaction. This comparison supports, once more, the opinion that the $\gamma/$ fibrous particles can not have been formed by any solid-state mechanism but must have originated from a solidification reaction.

The results given for samples S_{1.2} and S_{1.3} show that increasing powder and power feed rate causes significant melting of the steel substrate and brings about an increase in the maximum total thickness, the width of the coating, the hardness and the depth of the coating (Table 3). However, increasing the power and the powder feed rate also produced a microstructure containing refined dendrites and interdendritic phases (Table 3). The primary phases were then seen to become relatively more coarse, which means increasing the power and powder feed rate leads to a tendency for the microstructures to coarsen (Fig. 1.b). The XRD results for sample S_{1.3} reveal the effect of PTA processing parameters on the phases present in the coating microstructures using FeCrNi powders, as shown in Fig. 3.

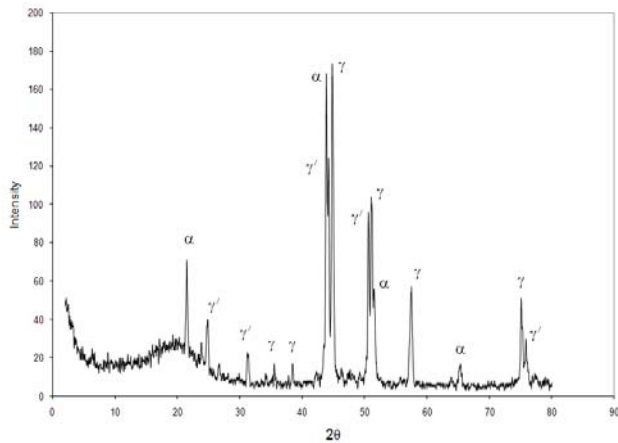
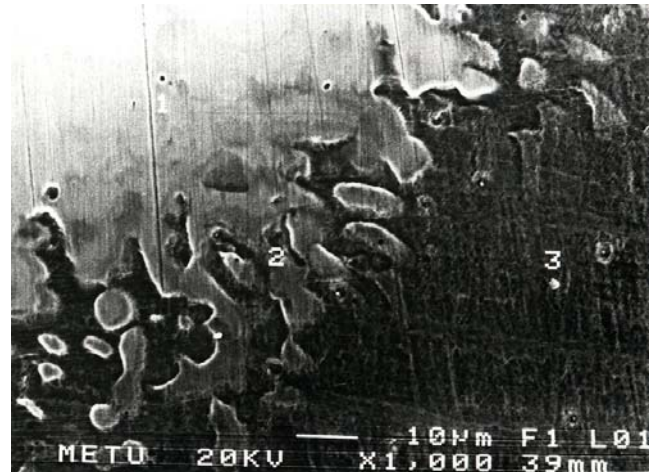


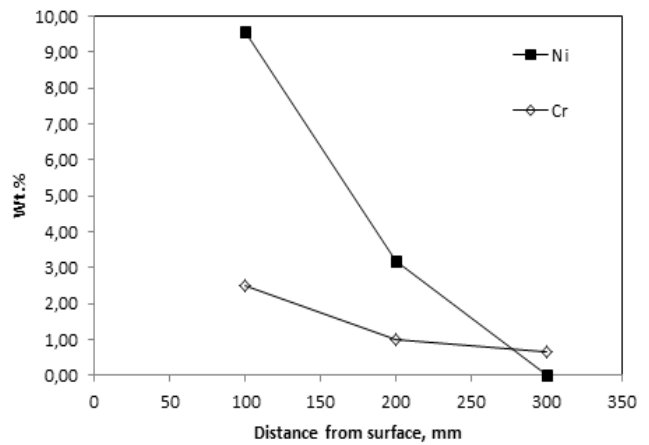
Fig. 3. XRD results of the sample $S_{1,3}$.

The presence of CrFeNiSi diffraction peaks is clearly visible, indicating the formation of CrFeNiSi in an austenite (γ) phase. The EDS analyses of the hard phases for sample $S_{1,3}$ show that the Fe/Cr ratio is in the range of 2.34-3.14. The hardness of the CrFeNiSi increased with an increase in the Cr content of the intermetallics (Fig. 2). The relationship between the Cr content and CrFeNiSi hardness provides an insight into the abrasion performance of the coated surface [15]. Put very simply, a higher Cr concentration produces harder CrFeNiSi [15-18] (Table 3). It can also be seen from the EDS analyses that the hard phases contain more than 3wt.%Mn (Fig. 2). On the other hand, the matrix of a coated surface loses its Mn content, dropping to 5wt.%. The diffusion of Mn from the matrix to the carbide is attributed to the solidification sequence that occurs during coating.

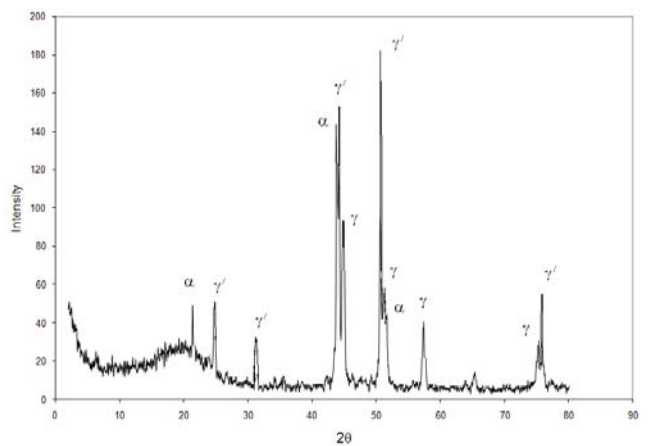
Microstructural investigations of the second group of samples show the formation of primary γ phases (Fig. 4) in which changes in chemical composition of superficial layers occur. The EDS analyses of the carbide and matrix of the samples coated by NiCr alloy powders are depicted in Fig. 4b. The chemical analyses were performed on portions of material taken from the centre of the coated surface plate. The micrograph shows that the phase structure is of a eutectic type. The visible intermetallic phases are in dendritic form (approximately 10 μm) and the matrix is in interdendritic form. The resulting CrFeNi intermetallics can be abbreviated as Cr_2FeNi based on the Fe/Cr ratio (Fig.4) [19]. The analysis reveals that the major phase in the microstructure of $S_{2,3}$ is austenite (γ) and the minor phase is (Cr_2FeNi). An increase in the feed rate of the NiCr powders to the coating powders mixture raised the vol.% and the size of the intermetallic phases. This is thought to be due to an increase in the eutectic temperature caused by the presence of Ni in the coating substrate.



(a)



(b)



(c)

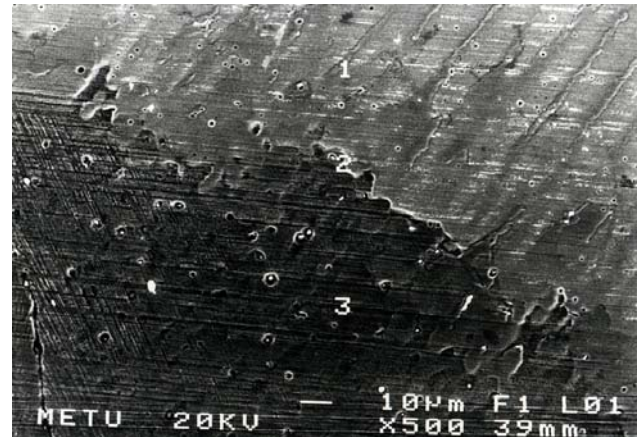
Fig. 4. a) Microstructure of sample $S_{2,3}$, b) EDS analyses of the matrix of the sample $S_{2,3}$ depicted in Fig. 4a, c) XRD of the sample $S_{2,3}$.

In the Ni-Cr diagram, two solid phases exist. The Mn-Cr diagram, however, shows three solid phases, as a σ phase can also be formed. The NiMn-Cr diagram, however, will be σ -safe, as σ formation is calculated to occur at much higher Mn concentrations [20]. In the Ni-NiAl diagram, three solid phases exist. The Mn-NiAl diagram, however, shows only two, as γ -Ni₃Al becomes unstable and will not normally be formed as soon as 1/3 of the Ni is substituted by Mn [21]. The solidification relies on a long-range diffusion-controlled process. It is slower than the solidification of ordered alloys, which solidify in a short-range order-controlled process. The growth rate of the solidification reaction can be calculated using Eq. (1) [22]. This equation is:

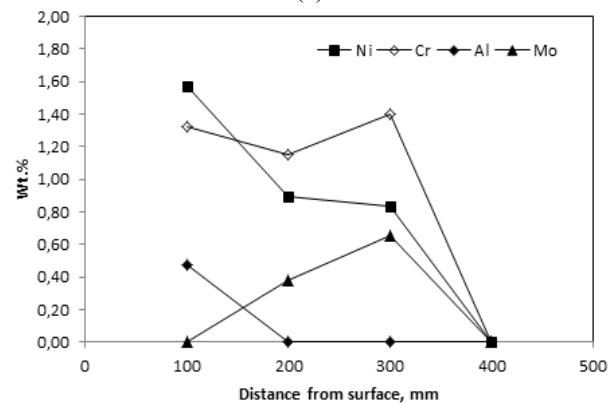
$$\lambda^2 v \Delta C^2 D = 1.9 \times 10^{-12} \text{ cm}^5 \text{ s}^{-2} \text{ at\%} \quad (1)$$

where λ is the interphase spacing, or the distance between the phase particles (lamellae or fibres) of the same phase, in cm; v is the solidification rate in cm/s; ΔC is the concentration difference at the actual solidus temperature; D is the inter-diffusion coefficient in the liquid state (commonly taken as 10^{-5} cm²/s). Eq. (1) will give a result of approximately 5-20 mms⁻¹ for a λ value of 0.05-0.1 μ m. This value compares reasonably well to the maximum growth rate for similar lamellar of 25 and 8 mms⁻¹. The spacing at high solidification rates will be controlled by a change in the mechanisms of local equilibrium that depend on liquid-solid interface curvature and differences in actual diffusion. The $\lambda^2 v$ value increases when the $\lambda v/2D$ becomes large with respect to unity at high growth rates. The $\lambda v/2D$ in this study is estimated to be close to 0.1. This estimate is based on the high "DC" value of 60 at%, as well as on the rejection of ternary elements from the terminal phases. However, this model can not conclusively explain the broad variation in λ in this special case, which is a factor of two, but it may give a hint to a possible explanation. This model may also account for the effective " $\lambda v/2D$ " not being constant, but this also depends on different terms, e.g. segregation, variations in undercooling and concomitant supersaturation. The γ Ni seems to tolerate the substitution by Mn, because Ni and Mn are chemically similar and both have extensive solid solubility with Cr, so it is possible that these elements can not be "distinguished" from each other during rapid solidification.

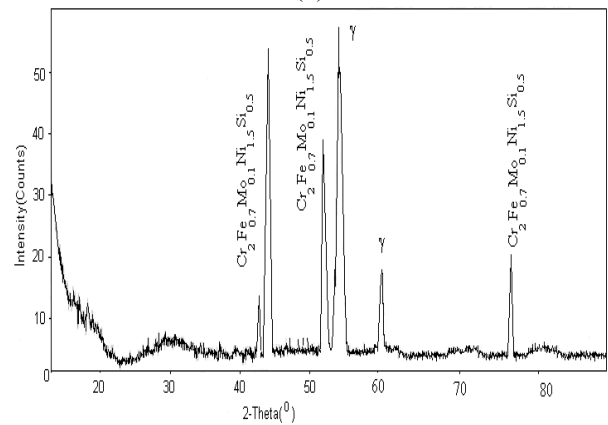
FeNiAlMo powders were used to coat a third group of samples. The coating thickness, hardness and production parameters for samples S_{3,1}, S_{3,2} and S_{3,3} are given in Table 3. The stability of the matrix is important during the wear process [23] so it was thought that Ni addition would decrease the chemical potential energy of the austenite phase, and form NiAl intermetallics and CrFeNiSi intermetallics. Figure 5 shows that NiAl powder promotes the formation of refined dendrites and an interdendritic eutectic, unlike the microstructure of the S₁ and S₂ sample groups. Consequently, the size and quantity of the intermetallics at the coated surface decreased with FeNiAlMo powders (Fig. 5).



(a)



(b)



(c)

Fig. 5. a) Microstructure of sample S_{3,3}, b) EDS analyses of the matrix of the sample S_{3,3} depicted in Fig. 5a.

Furthermore, an increase in the powder feed rate and heat input caused structural changes. The results obtained for samples S_{3,2} and S_{3,3} are depicted in Table 3, which confirms that the increase in the powder feed rate and the heat input produced grain refinement and enhanced microhardness. Fig. 5 notes the change in chemical composition of the superficial layer and the EDS analyses of the intermetallics and matrix. The resultant intermetallic phases of the S₃ group samples can be abbreviated as CrFeNi from the Fe/Cr ratio (Fig. 5b) [24].

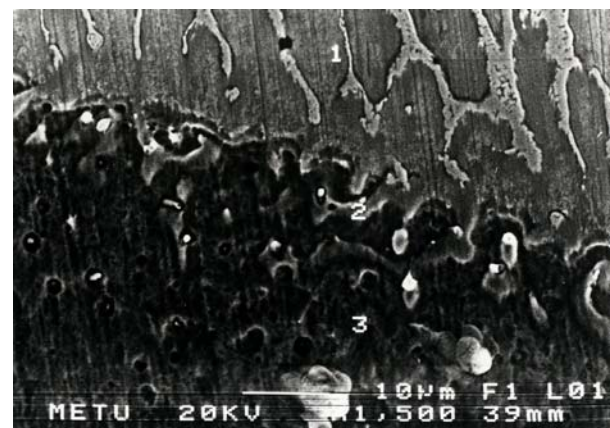
The microstructural results of the third group reveal the occurrence of two basic structures, both of which depend on the PTA processing parameters and the associated alloy compositions. Microstructural changes occur in the primary dendrites of γ (fcc), and the eutectic results as the formation of a hcp CrFeNi intermetallic in the γ phase. This analysis reveals the effect of Ni-Al-Cr on the phases present in the surfaces of the coating microstructures (such as an increase in the intensity of the austenite phase).

The mechanism of the second structure involves the formation of NiAl and eutectic γ . The XRD results also confirm that the addition of Ni leads to the formation of eutectic structures containing austenite and a CrFeNi phase mixture with NiAl. The segregation of this reinforcement contributes to a reduction in the secondary dendrite arm spacing (Fig. 5a). In contrast, an increase in the FeNiAlMo feed rate refined the size of the CrFeNi, modified connectivity and the decreased volume fraction of CrFeNi (Table 3). The refinement of the structure with the addition of NiAl is thought to be due to a change in the solidification range. The microstructure of the base iron (FeCrMn) is hypoeutectic, but the presence of Ni in the microstructure moved the chemical composition of the alloy closer to the eutectic composition and eventually into the hypereutectic region.

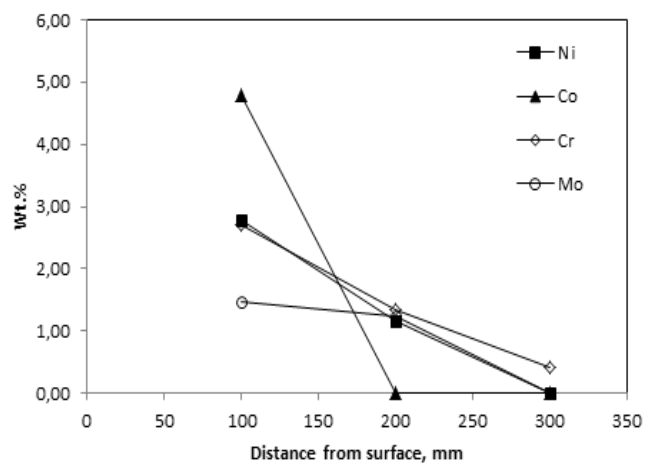
In the eutectic composition the solidification range is shorter; and the shorter the solidification range, the finer the structure of the alloy obtained will be. In the microstructure, eutectic grains (γ/γ' grains) were seen instead of single-phase. The volume fraction of γ' is approximately 45%. A lamellar structure will form if the minor phase is above 28 vol.%. The occurrence of fibrous instead of lamellar structures at approximately 45 vol.% was observed, which is in direct analogy in the fibrous NiAl-Cr eutectic if it was properly alloyed with Mo for a zero lattice misfit adjustment [25]. In either case, both phases have a nearly perfect atomic fit, as also suggested by the absence of dislocation networks at the γ/γ' interfaces. Thus the interface energy becomes independent of orientation relationships along the fibre interfaces, and thus favours fibrous structures. The γ phase essentially contains more than 60 at% Cr, the remainder being Ni and Mn. A large difference in the ease of crystallization from the Ni-Mn-Cr-Al melt becomes apparent in both eutectics in a similar manner because the bcc and fcc phases crystallize at different growth rates. Although bcc phases are nucleated from the melt more easily than the fcc (and hcp) phases, because of lower interface energies between the growing crystals and the melt the growth of the fcc phases over the bcc phases is kinetically favoured at any solidification rate; in any case, FCC crystals grow quicker. As the coupled growth of regular structures relies on the nucleation of one phase by the other, it is concluded that γ is crystallizing slightly ahead of the other phases. γ (=unordered solid solution) will allow γ' (=ordered crystal structure) to crystallize subsequently on it. At low solidification rates, however, γ' turns out to be unstable. Instead, the bcc α -Cr phase will be formed. Both γ and α

are unordered solid solutions that establish coupled growth via a random collision-limited process. The growth of the ordered β phase is short-range order dominated, which means that it is slower than a collision-limited process, and so its crystallization rate is too sluggish to crystallize competitively on γ as long as other more appropriate phases, like α , are present. This again suggests that the β phase does not form a continuous phase, but is somehow formed subsequently in a three-phase microstructure. Simultaneous crystallization of the three phases from the melt should be mandatory for the ternary case.

CoNiCrMo powders were used to coat the fourth group samples. The coating parameters are interpreted in Table 3. It was thought that the CoNiCrMo addition increased the chemical potential energy of the austenite phase, and formed CrFeNi intermetallics. Fig. 6 shows that CoNiCrMo powder promotes the formation of refined austenite dendrites and the interdendritic intermetallic phase. Consequently, the size and quantity of the intermetallics at the coated surface decreases with CoNiMo powders (Fig. 6).



(a)



(b)

Fig. 6. a) Microstructure of sample $S_{4,3}$, b) EDS analyses of the matrix of the sample $S_{4,3}$ depicted in Fig. 6a.

The presence of Ni, Co, Cr and Mo in alloying powders leads to a lamellar microstructure consisting of three phases, as shown in Fig. 6a. The dominant lamellar phase is γ -Ni (medium gray), the thinner lamellae are α -Cr (bright), and embedded in the α -Cr phase are β -NiAl particles (dark). The volume fraction of the lamellar structures determined by metallographic intersection method is 68 vol.% for the γ -Ni lamellae and 32 vol.% for the composite lamellae of the α + β phases. This raises the question of why a lamellar structure has been stabilized instead of a fibrous one, as the minor phases α and β are each less than 28 vol.%, in which, according to the rule, fibrous structures should be likely to form. The β -NiAl and the α -Cr phases are both arranged in a single lamella. If both phases are taken together, they represent a volume fraction in the order of 32%; the remainder being 68% of γ , and thus conform to the rule of eutectics. It is likely that both the α and β phases can be considered to have grown as one lamellar composite element. They apparently behave like a phase mixture on coupled growth with γ . It can be argued that the lamellae composed of α and β might have originally formed as α , with the β forming behind the liquid/solid interface in the solid state.

However, there are some objections to this type of solid state formation. First, the involvement of only two phases, α and γ , would again be inconsistent with the rule of eutectics that would indicate the formation of a fibrous eutectic for this case. Secondly, there is a full analogy to the binary Ni-Cr structure for this case regarding the identical phases of α and γ , and the type of coupled growth in which both phases solidify as lamellae [26]. The main difference noted between these systems concerns the processing. This difference in the solidification rate can partly be attributed to the heat input. It is also a strong argument for the simultaneous in situ formation of an aligned structure consisting of three phases. The task of establishing the proper arrangement of three phases is much more difficult than for a two-phase structure, and hence needs extremely slow solidification rates. The control of four diffusing elements instead of two also needs much more time. A precipitation reaction for β also seems unlikely. The arrangement of the α and β phases suggests a peritectic-like reaction to have taken the place of the type $L+\alpha=\beta$ instead (this means that α will exist first followed by β on solidification.). A transient reaction type of that kind may also be considered to be the case for α and β formation within the compound lamella. The interlamellar spacing between identical lamellae is 12 μm according to cross-sectional evidence. For a λ value for the eutectic of 12 μm and a solidification rate of 1.7cmh^{-1} ($=4.72\times 10^{-4}\text{cms}^{-1}$) approximately $DC=17\%$ is obtained using Eq. (1). This value represents the concentration difference between the two (hypothetical) contacting phases on coupled growth of α and γ . Different growth behaviours of respective phases then become more apparent, in which the γ phase exhibits unimpeded preferential unidirectional growth along the thermal gradient, and the α and β phases form a tattered α/β composite structure. It can not be decided categorically

whether the formation of the α or β phase has come first in this lamella escorted by γ lamellae, but the reaction scheme of $L+\alpha=\beta$ mentioned above suggests a ranking for the respective phases in terms of their ease of control that runs: $\gamma>\alpha>\beta$.

Microhardness measurements were performed through the thickness of the sample, to study the changes in the mechanical properties of the matrix due to plastic deformation by varying the distance to the contact surface. The microhardness distribution measurement method was used to determine the depth of the coatings. The variation of the microhardness for samples S_1 and S_3 across the transverse cross-section of the coating microstructures are shown in Fig. 7.

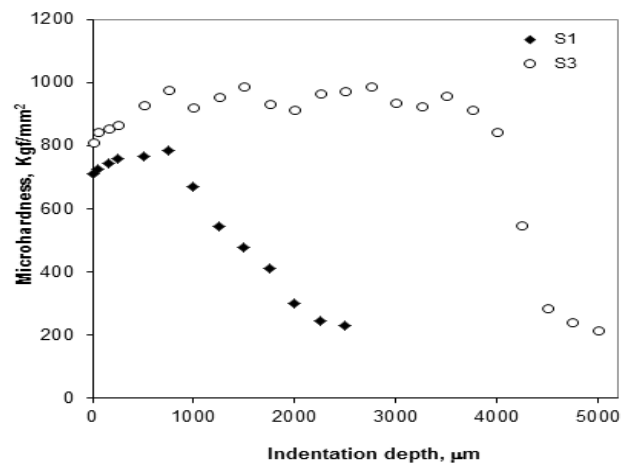


Fig. 7. The variation of the microhardness for sample $S_{1,3}$ and $S_{2,3}$ across the transverse cross-section of the coating microstructures.

The hardness profiles confirm that significant surface hardening was achieved using the PTA process. The microhardness shows a sharp fall at the boundary. The variations ranging from 800-1000 HV for sample S_3 should be attributed to the presence of large carbides in the microstructure (Table 3) that cause the alloyed layer to resemble a composite material. Conversely, the hardness profile of the refined microstructure of sample $S_{3,3}$, which was obtained at a much lower powder feed rate and heat input, exhibits fewer variations in hardness. The nature of the gradients of the hardness profiles at the interfacial regions suggests the existence of a narrow heat-affected zone, which is an inherent characteristic of the PTA surface process. It is known that the eutectic microstructures, the size of the dendrites and the spacing between their phases all depend on the solidification rate [27]. In addition, dendritic structures can form at relatively lower solidification rates. Therefore, the higher hardness of the sample $S_{2,3}$ is attributed to the formation of hard CrFeNiSi in the eutectic. On the other hand, the lower hardness of $S_{1,1}$ may be associated with a high ratio for the austenite phase in the primary dendrites. The results for samples $S_{1,1}$, $S_{1,2}$ and $S_{1,3}$ are compared in Table 3, which

shows that a marked enhancement of the coating hardness occurs due to the microstructural refinement.

3.2. Wear tests

The mechanical and tribological properties of the coatings depend strongly on the type of solidified phases, grain size, distribution of hard phases, and alloying concentration [6]. Fig. 8a shows the wear rate for samples S_1 , $S_{1,3}$, $S_{2,3}$, $S_{3,3}$ and $S_{4,3}$, in addition Fig. 8b shows the wear rate of $S_{1,1}$, $S_{1,2}$ and $S_{1,3}$ as a function of sliding distance. It can be seen that the FeCrNi alloying powders have a systematic effect on the wear rate of coated surfaces, irrespective of load. Similar wear rates (Fig. 8b) were also found for the samples created using NiCr-FeNiAlMo-Co alloying powders.

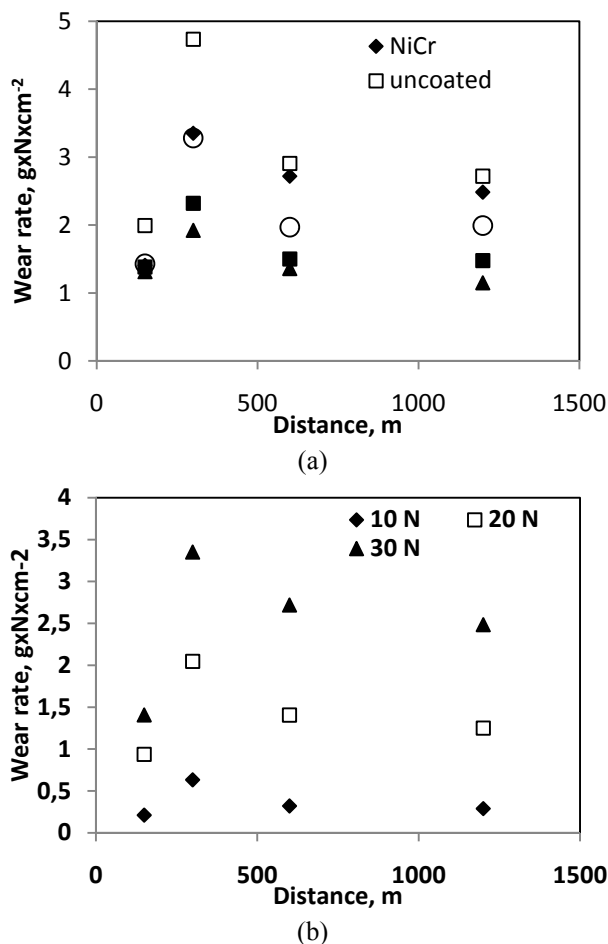


Fig. 8. a) The wear rate of samples S_1 , S_2 , S_3 , S_4 and S_5 under the load of 30 N, b) The wear rate of $S_{1,1}$, $S_{1,2}$, and $S_{1,3}$ as function of sliding distance.

The sample coated by FeCrNi alloying powders exhibited the lowest wear rate at each load. In contrast, the reference sample (uncoated) exhibited the greatest wear rate, followed by the surface coated using NiCr. The variation of the microhardness of FeCrC, FeW-FeCrC and FeW-FeCrC-NiAl coated samples with wear rate are interpreted in Fig. 9, where it is detected that the

relationship between microhardness and the wear rate is in the form of a power law expression:

$$W = ke^{nH} \quad (2)$$

Where W is the wear rate, H is the hardness, k is the wear coefficient, and n is defined as the wear exponent.

In addition, the hardness profiles demonstrate that significant surface hardening has been achieved by PTA processing (Fig. 6). From Fig. 9, it can be concluded that the increase in the powder feed rate increases the vol.% of intermetallic phases, hardness and decreases the wear rate by a considerable amount. The results demonstrate that the wear rate of the samples coated by FeNiAlMo powders is the most sensitive to the hard phase volume percentage of the coated surfaces.

The effects of load on the total wear rates of the samples are plotted in Fig. 10. The wear rates of the coated surfaces, which can also be called MMC composites, increase linearly through the entire applied load range, and they show that the change of wear rate against sliding distance takes the form of a polynomial function.

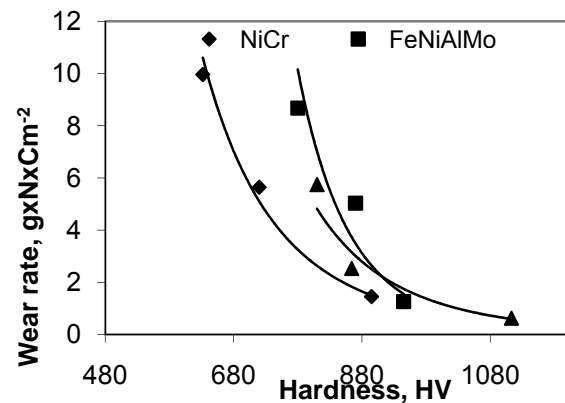


Fig. 9. The variation of the microhardness of coated samples with wear rate.

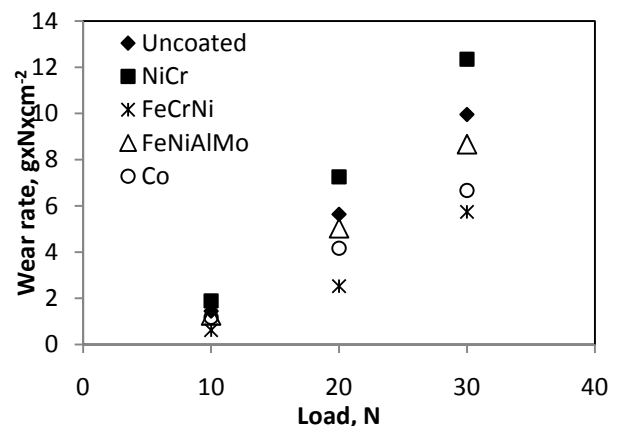


Fig. 10. The effect of the load on the total wear rates.

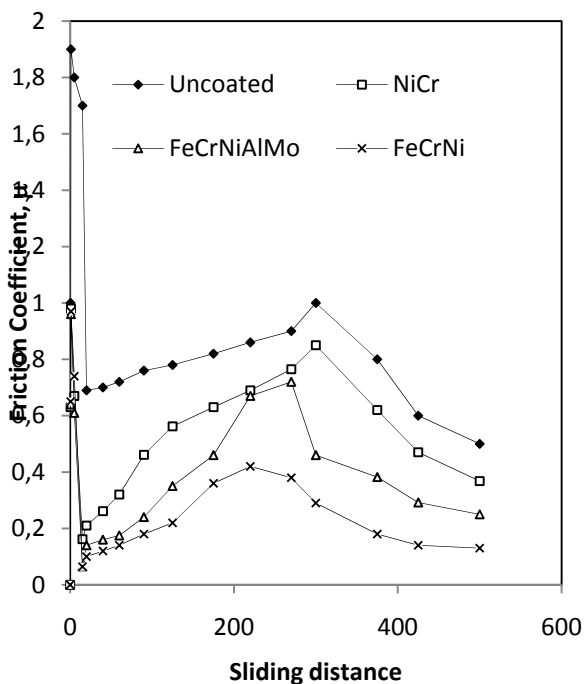


Fig. 11. The change of friction coefficient versus sliding distance of the samples.

Fig. 11 shows the friction coefficient (μ) for samples $S_{1, S_{2.3}, S_{3.3}$ and $S_{4.3}$, for a 1.8 m/min sliding speed. The friction coefficient increased from its initial value to a steady state after 300 m sliding. The friction reduced according to the alloying type, being 1 for the uncoated reference sample and 0.1 for the FeCrNi-coated samples. The alloyed surfaces increased friction slightly at all loads. The transition from mild to severe wear occurs when a critical temperature is reached at the contact surface as a result of frictional heating [9]. However, the severe wear was not seen for the tested conditions. The wear and friction data demonstrate that the microstructure and wear response are sensitive to small changes in the powder feed rate and powder type. It is interesting that the friction coefficient of the samples, especially samples S_1 and $S_{4.3}$, decreased as sliding distance increased. This suggests that the austenite phase is destabilized during the wear process close to the surface. The combination of high surface strain and temperature rises can promote the transformation of austenite to martensite. On the other hand, the current results suggest that it is the fragmentation of the intermetallics that controls the wear rate for coated samples.

The wear mechanism was found to be prevalently oxidative at all loads for all samples, although the metallic component ratio was increased by an increase in the load. This study has not discovered any apparent differences in wear surface morphology as a function of coating composition. An increase in load to 80 N resulted in higher wear coefficient, and higher degrees of wear and tear. The morphology of the wear debris was probably of delaminated oxides. At higher loads, the worn surface structure changed but abrasive grooving was not found,

and it is thought that local adhesion could be indicative of the roughening of the surface.

4. Conclusion

A ranking for the ease of solidification of a three phase structure in a Ni-Mn-Cr-Al melts runs $\gamma > \beta > \alpha$. FCC phases solidify quicker than BCC phases. The control of regular growth of β -NiAl is critical, while the solidified NiMnCrAl fibrous microstructure is exclusively formed of FCC phases γ and γ' , and is devoid of BCC α and β . Metastable FCC γ' phase fibres are preferred at the expense of stable BCC α and β . Ternary and quaternary elements will be rejected from the γ and γ' phases, and extended solid solutions with properly-sized partner atoms will be established instead, regardless of thermodynamics.

Coating dimensions and hardness have changed according to the process parameters and powder type. Increases in the power and the powder feed rate produced a microstructure with refined dendrites and interdendritic phases. The major phase in the microstructure of $S_{2.1}$ is austenite (γ), and the minor phase is (Cr_2FeNi) . An increase in the feed rate of the NiCr powders to the coating powders mixture raised the vol.% and the size of the intermetallic phases. The hardness of the CrFeNiSi increased as the Cr content of the intermetallics increased. The size and quantity of the intermetallics at the coated surface decreased with FeNiAlMo powders. The powder feed rate and heat input produced grain refinement and enhanced microhardness. The addition of Ni leads to the formation of eutectic structures containing austenite and CrFeNi phase mixture with NiAl. CoNiMo addition increased the chemical potential energy of the austenite phase, formed CrFeNi intermetallics, promoted the formation of refined austenite dendrites in the interdendritic intermetallic phase, and decreased the size and quantity of the intermetallics.

The variations in the microhardness of coated samples according to the wear rate revealed that their relationship is in the form of a power law. In addition, the wear rate curves demonstrate that the wear rate (W) changes with the surface temperature and the load, also in power law as expressed in eq (1). The friction coefficient was changed in the power law up to severe wear. But taking account of the mild and severe wear together, it was seen that friction coefficient and sliding distance changed according to a polynomial function. The increase in the powder feed rate increased both the hard phase vol.%, and friction coefficient. Among the samples, the lowest wear rate was obtained from the samples coated by FeCrNi coating alloy powders.

References

- [1] R.L. Deuis, J.M. Yellup, C. Subramanian, *Compos. Sci. & Technol.* **58**, 299 (1998).

- [2] E. Bourithis, A. Tazedakis, G. Papadimitriou, *J. Mater. Process. Technol.* **128**, 169 (2002).
- [3] M. Yan, *Surf. & Coat. Technol.* **99**, 132 (1998).
- [4] T. Teker, S. Karataş, S. O. Yılmaz, *J. Optoelectron. Adv. Mater.* **15**(3-4), 284 (2013).
- [5] Y. F. Liu, J.S. Mu, X.Y. Xu, S.Z. Yang, *Mater. Sci. & Eng. A.* **458**(1-2), 15366 (2007).
- [6] S. Schreck, K.H. ZumGahr, *Appl. Surf. SCI.* **247**(1-4), 15, 616 (2005).
- [7] S. Akgün, S. Sahin, F. Ustel, *Mater. Manuf. Process.* **24**, 909 (2009).
- [8] A. Matthews, A. Leyland, K. Holmberg, H. Ronkainen, *Surf. & Coat. Technol.* **100-101**, 1 (1998).
- [9] W. Xiaolei, C. Guangnan, *Mater. Sci. & Eng. A.* **270**(2), 183 (1999).
- [10] M. Abu-Aesh, *Mater. Manuf. Process.* **23**, 726 (2008).
- [11] M. Zapponi, A. Quiroga, T. Pe´rez, *Surf. & Coat. Tech.* **122**, 18 (1999).
- [12] P. Rogl, in: G. Petzow, G. Effenberg (Eds), *Ternary Alloys*, Vol. 4, Wiley-VCH, Weinheim, pp. 400, 1991.
- [13] M. Barth, *Dissertation, Ruhr-Universitat Bochum*, 1995.
- [14] S.O. Yılmaz, *J. Mater. Sci.* **42**, 6769 (2007).
- [15] C.S. Han, C.H. Bae, J.H. Lee, *Met. Mater. Int.* **15**(6), 891 (2009).
- [16] J. Zhang, A.T. Alpas, *Mater. Sci.& Eng. A.* **160**(1), 15, 25 (1993).
- [17] A. Frenk, W. Kurz, *Advanced techniques for surface engineering*, Dordrecht, The Netherlands, 1992.
- [18] G. Laird, R. Gundlach, K. Rohrig, *American Foundry Society, Des Plaines, Illinois*, 2000.
- [19] L. Kaufman, H. Nesor, *Met. Trans.* **6A**, 2115 (1975).
- [20] M. Hubert-Protopopescu, H. Hubert, in: G. Petzow, G. Effenberg (Eds.), *Ternary Alloys*, Vol. 4, Wiley-VCH, Weinheim, , pp. 234, 1991.
- [21] S.R. Chen, H.A. Davies and W.M. Rainforth, *Acta Mater.* **47**(18), 4555 (1999).
- [22] D. Gorscak, T. Filetin, and D. Cackovic, *Mater. Manuf. Process.* **24**, 828(2009).
- [23] K.A. Jackson, J.D. Hunt, *Trans. Metall. Soc. AIME.* **236**, 1129 (1966).
- [24] S. Gnyusov, S. Tarasov, Yu. Ivanov, V. Rothstein, *Wear.* **257**, 97 (2004).
- [25] R. Kossowsky, W.C. Johnston, B.J. Shaw, *Trans. AIME.* **245**, 1219 (1969).
- [26] R. Trivedi, W. Kurz, *Proc. Symp. Solidification processing of eutectic alloys, TMS-AIME*, Warrendale, PA, pp. 3-34, 1988.
- [27] I. Karaman, H. Sehitoglu, K. Gall, Y.I. Chumlyakov, H.J. Maier, *Acta Mater.* **48**(6), 1345 (2000).

*Corresponding author: tteker@adiyaman.edu.tr